Measurements of electron-impact ionization cross sections of neon by comparison with photoionization

A. A. Sorokin, L. A. Shmaenok,* and S. V. Bobashev
A. F. Ioffe Physico-Technical Institute RAS, Politekhnicheskaya 26, 194021 St. Petersburg, Russia

B. Möbus and G. Ulm
Physikalisch-Technische Bundesanstalt, Abbestrasse 2-12, 10587 Berlin, Germany
(Received 10 April 1998)

A method and apparatus have been developed for precise measurements of the ratios of total cross sections for electron-impact ionization and photoionization in rare gases based on the comparison of the total ion yields of the two ionization processes. Low uncertainties for the cross-section ratios are achieved above all by using a cryogenic electrical substitution radiometer as a primary detector standard in the soft-x-ray and vacuum ultraviolet spectral ranges in order to determine the impinging photon flux. On the basis of our measured cross-section ratios and well-known total photoionization cross sections we deduce absolute total electron-impact ionization cross sections of rare gases. As a result we present ratios of total electron-impact ionization cross sections to total photoionization cross sections and deduce total electron-impact ionization cross sections of neon in the energy range of electrons from 140 to 4000 eV and of photons from 100 to 1500 eV. Relative uncertainties as low as 1.3% for the cross-section ratios and 2.8% for the total electron-impact ionization cross sections have been achieved. A comparison of our cross-section data with published experimental and theoretical data is presented. [S1050-2947(98)05310-4]

PACS number(s): 34.80.Dp

I. INTRODUCTION

Electron-impact ionization and photoionization are two fundamental processes in atomic and molecular physics. The knowledge of absolute total and partial cross sections for these processes with low uncertainties is crucial for the precise understanding of the dynamics of electron-atom and photon-atom interactions. Moreover, these data play an important role in many fields of applied research and modeling covering discharges and plasmas, controlled nuclear fusion, eximer lasers, planetary, and stellar atmospheres.

Electron-impact ionization (EI) of atoms and molecules has been extensively investigated by various groups since the 1930s (see the reviews [1–3] and references therein). At present, rare gases, for which total [4–10] and partial [7–13] EI cross sections [14] were measured in a wide energy range, are the most popular targets. Nevertheless, even for these simple species the situation as regards accurate cross-section data is still far from being satisfactory. Although quoted relative uncertainties of measured cross sections typically range from 6% to 10%, results obtained by some groups differ by up to 25% [1,2]. To our knowledge, there is a single experimental work [10] in which EI cross sections were obtained (for argon only) with quoted relative uncertainties as low as 3.5%.

As shown in reviews [1–3], the main contributions to the experimental uncertainties of EI cross sections arise from the absolute measurements of (a) the number of impinging electrons, (b) the number of ions created, (c) the interaction path length accepted from the ion detector, (d) the detector efficiency for differently charged ions, and (e) the target gas density at a pressure of less than 10^{-2} Pa, which is typical of EI experiments.

In the case of total *photoionization* (PI) cross sections, the application of both the absorption cell technique and the double ionization chamber technique allows most of the problems (a) to (d) to be avoided [15]. Moreover, due to a gas pressure in the order of 100 Pa used in these techniques, the application of precision oil manometers and capacitor manometers has made it possible to reduce the relative uncertainty of the target gas density to less than 1% [16]. As a result, at least the total PI cross sections of rare gases are presently known with relative uncertainties as low as 1% to 3% [16–21], i.e., with uncertainties significantly better than those achieved for EI.

We report here a method for the determination of total EI cross sections of rare gases, which is based on the accurate measurement of ratios of total cross sections for EI and PI. For the practical application of this method we developed an ionization chamber in which the total ion yields by photon and by electron impact are compared by applying the main principles demonstrated earlier in [22]. Using photodiodes calibrated against a cryogenic electrical substitution radiometer (ESR) (the primary detector standard in the soft-x-ray region, which substitutes the incident radiant power by electrical power, which can be measured with low uncertainty), the impinging photon flux can be measured with relative uncertainties below 1% [23,24]. Based on this progress achieved in measurements of the photon flux and of the ion yield ratios, we measured ratios of total cross sections for EI and PI with a relative uncertainty as low as 1.3%. (All uncertainties concerning our experiment are 1σ values.) Our relative measurements eliminate the main sources of uncer-

*Present address: FOM–Institute for Plasma Physics, Edisonbaan 14, 3430 BE Nieuwegein, The Netherlands.

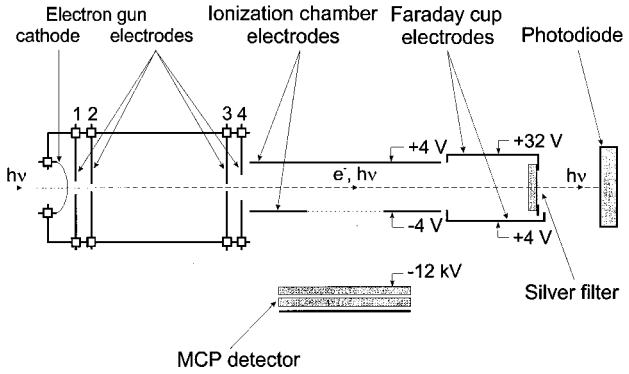

FIG. 1. Schematic diagram of the apparatus.

tainties in absolute total cross-section measurements and yield a common scale of total cross sections for EI and PI. Using our measured cross-section ratios and well-known PI cross sections (see the Appendix), we deduce absolute total EI cross sections of rare gases with unparalleled low relative uncertainties (below 3%). Our results considerably improve the data base for absolute total EI cross sections and hence for partial cross sections derived from these data.

As a result, we present in this paper ratios of EI and PI cross sections and absolute total EI cross sections for neon in the energy range of electrons from 140 to 4000 eV and of photons from 100 to 1500 eV. In addition, we compile the PI cross-section data of neon already available and give values recommended for them in the spectral range from 70 to 2000 eV.

II. APPARATUS AND EXPERIMENTAL METHOD

The measurements were performed at the SX700 beam line in the radiometry laboratory of the Physikalisch-Technische Bundesanstalt at the electron storage ring BESSY I. The beam line is equipped with an SX700 plane grating monochromator and a toroidal refocusing mirror behind the exit slit of the monochromator. It is optimized for high spectral purity and intensity of the radiation. Within the photon energy range from 40 to 1500 eV the resolving power $\lambda/\Delta\lambda$ ranges from 400 to 3000. A photon flux of up to 10^{11} s^{-1} is available. The fraction of stray light and higher-order radiation is smaller than 1% [25].

The apparatus used for cross-section measurements consists of an ionization chamber, an ion detector, an electron gun, a Faraday cup for electron current measurements, and a photodiode, calibrated against the ESR, for photon flux measurements (Fig. 1). All elements are mounted in a stainless-steel vacuum chamber evacuated by a turbomolecular pump to a residual pressure of 1×10^{-5} Pa. Neon of 99.99% purity is introduced into the chamber via a needle valve. Its pressure is kept at certain levels in the range between 8×10^{-4} Pa and 7×10^{-3} Pa during the measurements. A differential pumping unit is used to separate the beam line at ultrahigh vacuum from the apparatus.

The operation of the apparatus is based on the consecutive ionization of neon by electrons and photons. In the first step, a beam of monoenergetic electrons of energy E generated by the electron gun is directed between two parallel stainless-steel electrodes of the ionization chamber and collected in the Faraday cup. An electric extraction field maintained perpendicular to the electron beam drives positive ions toward the bottom electrode. Through an aperture (3.4×3.4 cm^2) in this electrode, which is covered by a nickel electroformed grid, a fraction of the ions enters the gap between the bottom electrode and the front of the microchannel plate (MCP) detector. Here the ions are accelerated towards the MCP detector, where they are finally registered. The ion extraction and accelerating fields are chosen to be high enough to obtain equal collection and detection efficiency for differently charged ions. Under these conditions the count rate f_e of the MCP detector is proportional to the number N_e of electrons per second in the electron beam and the total EI cross section $\sigma_e(E)$:

$$f_e = k_e N_e \sigma_e(E). \tag{1}$$

In the second step, the electron beam is ceased and a beam of monochromatized synchrotron radiation of photon energy $h\nu$ enters the ionization chamber through the hollow-axis electron gun, passes through an aperture in the bottom of the Faraday cup covered with a thin silver filter of known transmittance, and is detected by the photodiode. The ions created by PI are collected and registered as are the ions created by EI. The MCP detector count rate f_{ph} is proportional to the number of photons per second N_{ph} and the total PI cross section $\sigma_{\mathrm{ph}}(h\nu)$:

$$f_{\mathrm{ph}} = k_{\mathrm{ph}} N_{\mathrm{ph}} \sigma_{\mathrm{ph}}(h\nu). \tag{2}$$

The coefficients of proportionality k_e and k_{ph} are determined by the geometric dimensions of photon and electron beam, the target gas density in the ionization chamber, the ion collection, and the ion detection efficiencies.

Essential features of our apparatus are the hollow-axis electron gun and the thin silver filter of known transmittance at the bottom of the Faraday cup. This design ensures coincidence of the photon and electron beam positions and allows EI and PI measurements to be performed without any shifting of electron gun and Faraday cup. This leads to a close similarity of the conditions at EI and PI as regards the gas density and the electric potential distribution within the ionization chamber. In combination with the above-mentioned equality of ion detection efficiencies, it leads to identical conditions for the formation and detection of the ions, i.e., $k_e = k_{\mathrm{ph}}$ (for a detailed discussion see Sec. III).

N_e is determined through the Faraday cup current I_e by $N_e = I_e/e$, where e is the elementary charge, whereas the photon flux N_{ph} is determined by the photodiode current I_{ph}, the photodiode quantum efficiency $\eta_{\mathrm{ph}}(h\nu)$, and the transmittance $\tau_{\mathrm{ph}}(h\nu)$ of the silver filter:

$$N_{\mathrm{ph}} = \frac{1}{\tau_{\mathrm{ph}}(h\nu)} \frac{1}{\eta_{\mathrm{ph}}(h\nu)} \frac{1}{e} I_{\mathrm{ph}}. \tag{3}$$

Using this relation and taking into account that $k_e = k_{\mathrm{ph}}$, the ratio of the total EI cross section to the total PI cross section is expressed as

TABLE I. Contributions to the relative uncertainty (1σ level) of the ratios of the total cross sections for electron-impact ionization and photoionization of neon at 1000-eV electron energy and photon energies $h\nu$ ranging from 100 to 1500 eV.

	Contributions to the relative uncertainty of total-cross-section ratios (%)	
Source of uncertainty	100 eV$\leqslant h\nu \leqslant$700 eV	900 eV$\leqslant h\nu \leqslant$1500 eV
Current of the impinging electrons	0.2	0.2
Energy of the impinging electrons	0.1	0.1
Number of the impinging photons		
photodiode current	0.1	0.1
silver filter transmittance	0.2	0.2
photodiode quantum efficiency	0.8	0.8
Energy of the impinging photons	0.2	0.4
Count rate measurements		
counting statistics	0.5	0.5
background correction	0.1 to 0.4	0.2
linearity of detector	0.5	0.5
Equality of interaction path lengths	0.1	0.1
Equality of ion collection efficiencies	0.5	0.5
Equality of ion detection efficiencies	0.1	0.5
Gas pressure stability	0.1	0.1
Secondary effects	0.3	0.3
Second-order contribution	0.1 to 0.5	0.1
Stray light contribution	0.2	1.0
Total relative uncertainty (sum in quadrature)	1.3 to 1.4	1.7

$$\frac{\sigma_e(E)}{\sigma_{\mathrm{ph}}(h\nu)} = \frac{1}{\tau_{\mathrm{ph}}(h\nu)} \frac{1}{\eta_{\mathrm{ph}}(h\nu)} \frac{f_e/I_e}{f_{\mathrm{ph}}/I_{\mathrm{ph}}}. \tag{4}$$

The essence of the present experimental work is the accurate absolute measurement of all quantities on the right-hand side of this equation. In the following, we discuss in detail these measurements and the respective contributions to the total relative uncertainties of the cross-section ratios (summarized in Table I).

III. EXPERIMENTAL DETAILS AND DISTURBING EFFECTS

A. Electron current measurements

The electron beam is generated by an electron gun equipped with a directly heated 100-μm tungsten wire cathode. Electrons emitted from the cathode are accelerated through a system of knife-edged circular apertures in aluminum electrodes 1 to 4 (see Fig. 1). All electrodes are on ground potential, except the first, with an aperture 2.5 mm in diameter. During PI measurements, this electrode is biased in relation to the cathode to cut off the electron flow. Electron beam collimation is achieved by two 2-mm-diam apertures in electrodes 2 and 3, which are 16 cm apart. The slightly divergent electron beam passes through the 5-mm-diam aperture in electrode 4, travels approximately 9 cm between two parallel electrodes of the ionization chamber, which are 1.6 cm apart and maintained at constant potentials of $+4$ and -4 V, and finally enters the Faraday cup. The diameter of the electron beam is approximately 2.5 mm at the center of the ionization chamber and 3 mm at the entrance of the Faraday cup.

The Faraday cup is a rectangular parallelepiped 8 cm in depth, with an entrance aperture of 1.6×1.6 cm^2. It consists of two electrodes, one of which has an aperture at the backside of the cup 1 cm in diameter. This aperture is covered by a silver filter 0.25 μm thick, which is supported by a nickel electroformed mesh. The cup electrodes are held on potentials of 4 and 32 V. With this design, the primary electrons entering the cup are collected along with secondary electrons and ions, which are produced within the cup volume, resulting in currents at both cup electrodes. These currents are added, measured with a relative uncertainty of 0.1% using a calibrated Keithley 617 electrometer, and taken as the current I_e of the electron beam. Typical currents range from 50 pA to 2 nA.

Consistency checks proved that all electrons traversing the ionization chamber are collected in the Faraday cup. First, the measured cup current is independent of the potential applied to an additional 1-cm-diam aperture (not shown in Fig. 1) behind the silver filter, demonstrating that the silver filter is thick enough to absorb all impinging electrons. Second, to demonstrate the absence of secondary electrons escaping from the Faraday cup, the currents collected by the cup and by the ionization chamber electrodes are measured as a function of the cup potentials. Within a relative uncertainty of 0.2% no change of the electron current is observed for potentials at the Faraday cup higher than those mentioned

above and the total current collected by both ionization chamber electrodes is less than 0.2% of the electron current. Therefore, within a relative uncertainty of 0.2%, the collection efficiency for electrons entering the cup is 100%.

The loss of beam electrons between the interaction region observed and the Faraday cup may distort the electron current measurement. Elastic and inelastic scattering of electrons on target gas atoms is negligible at the gas pressures used. The loss due to electron deflection from a straight direction caused by electric and magnetic fields is also negligible. A high-permeability magnetic shield reduces the ambient magnetic field to approximately 40 mG, which has a negligible influence on the fast electrons used. The transverse electric field of 5 V/cm within the interaction region leads to a maximum beam deflection of about 7.5 mm at the entrance of the Faraday cup for 140-eV electron energy, decreasing with increasing electron energy. All electrons passing the interaction region therefore enter the Faraday cup.

The electron beam energy depends on the potential applied to the cathode of the electron gun and is determined with an absolute uncertainty of ± 1 eV, which results from the filament voltage drop at the cathode. A relative uncertainty of 0.7% at an electron energy of 140 eV is therefore the upper limit of the contribution to the total relative uncertainty of our cross-section measurements, decreasing rapidly with increasing electron energy.

Secondary electrons with energies ranging from a few eV to the primary electrons' energy, which are released from the material of the gun electrodes as a result of electron impact, may influence the spectral purity of the beam. To check the presence of such secondaries, we measure the dependence of the Faraday cup current on the electric field applied between the two ionization chamber electrodes for different electron beam energies. The current remains constant up to field values at which deflected primary electrons begin to hit the ionization chamber electrodes. From this we conclude that the fraction of secondary electrons in the beam is below 0.1%.

Finally, it should be noted that the potential configuration at the ionization chamber electrodes ensures the ground potential at the center between them so that a distortion of the electron energy within the chamber is negligible. Moreover, because ions are collected from the interaction region (see Sec. III C) at a distance of approximately 3.5 cm from the Faraday cup, which is twice the distance between the ionization chamber electrodes, the influence of the cup potentials on the electron beam energy is negligible too.

B. Photon flux measurements

The monochromatic photon beam with the photon energy $h\nu$ from the beam line is directed through the hollow-axis electron gun and traverses the ionization chamber along the same path as the electron beam, with a divergence of approximately 1.5 mrad and a focus size of approximately 2×1 mm^2 at the center of the ionization chamber [25]. After having passed through the silver filter at the back side of the Faraday cup, the photon beam is detected by a silicon *n*-on-*p* IRD AXUV 100 G photodiode with an active area of 1 cm^2. In a preceding calibration against an ESR [23,24], the quantum efficiency $\eta_{\rm ph}(h\nu)$ of this photodiode is determined with a relative uncertainty of 0.8%. The photodiode current $I_{\rm ph}$ is measured with a relative uncertainty of 0.1% by the same Keithley 617 picoamperemeter used to measure the electron current. Typical values of the photodiode current ranges from 50 Pa to 30 nA, depending on the photon flux and the transmittance $\tau_{\rm ph}(h\nu)$ of the silver filter. Since the Faraday cup is mounted on a linear motion feedthrough, it can be removed from the beam without breaking the vacuum. During our experiments, the transmittance of the silver filter can therefore be measured with a relative uncertainty of 0.2%. Finally, the uncertainty of the monochromator energy calibration leads to an additional relative uncertainty of 0.4% for the determination of the photon flux since $\eta_{\rm ph}(h\nu)\sim h\nu$.

C. Ion-yield measurements

EI and PI of neon produce singly and multiply charged ions within the interaction region between the two ionization chamber electrodes. A static electric field of 5 V/cm extracts a fraction of the ions through a (3.4×3.4)-cm^2 aperture in the bottom electrode. A bias voltage of 12 kV at the front of the MCP detector that is located 4 cm from the chamber axis additionally accelerates the ions; this results in a 12-keV impact energy on the detector for singly charged ions and twice that energy for doubly charged ions.

The MCP detector is a chevron-type assembly consisting of two microchannel plates, 56 mm in diameter, in front of a stainless-steel anode. The potential at the front of the MCP, a voltage of about 1 kV applied to each plate, and a bias of about 100 V between the last plate and the anode are provided by two power supplies and can be varied independently. The MCP detector output is coupled through a high-voltage capacitor to an Ortec 9301 preamplifier–Philips Scientific 771 amplifier combination with a gain of 1000. Its output is fed into a Canberra 2128 discriminator with a threshold level of about 1 V. The discriminator output pulses of 200 ns width and 2 V magnitude are recorded by an Ortec 974 counter. Typical values of the count rate range from 5 to 200 kHz depending on the electron and photon fluxes, the cross sections for EI and PI, and the target gas density. When an appropriate exposure time is chosen, the relative uncertainty caused by the counting statistics is always below 0.5%. Background ion signals associated with the ionization of the residual gas are subtracted from the total count rates, resulting in true count rates f_e and $f_{\rm ph}$. A relative uncertainty of 0.4% is the upper limit of the contribution of the background correction to the total relative uncertainty of our cross-section measurements.

As mentioned in Sec. II, identical conditions for the production and registration of ions created by EI and PI are essential for our measurements. Factors that may impede achieving this are considered below.

1. Linearity of the detector-amplifier-counter combination

Count rates are kept at almost equal levels during EI and PI measurements by proper adjustment of the beam intensities. However, in some spectral ranges these count rates may differ by a factor of 3. To test the nonlinearity of the detector-amplifier-counter combination, a dependence of the

count rate on both the electron and the photon flux is measured. The upper limit to the influences of nonlinearity is found to be 0.5%.

2. Equality of interaction path lengths

When the electron beam passes through the interaction region, it may be deflected from straightness by maximally 2.7 mm at an electron energy of 140 eV due to the presence of the transverse electric field. This may lead to an inequality of EI and PI interaction path lengths from which ions are collected by the MCP detector. The upper limit of the relative uncertainty caused by this effect is 0.3% at an electron energy of 140 eV, decreasing rapidly with increasing electron energy.

3. Equality of ion collection efficiencies

The equality of the total ion collection efficiencies for EI and PI may be disturbed by a possible dependence on the ion charge spectra. For EI of neon in the electron energy range from 140 to 4000 eV, the fraction of multiply charged (dominantly doubly charged) ions is approximately 4% to 6% (see, e.g., [13]). In the case of PI, this contribution is between 6% and 15% in the photon energy range below the 1*s* threshold of neon (~870 eV) and increases to 96% in the spectral range above the former (see, e.g., [26]). In addition, different ion recoiling occurs for EI and PI, resulting in a different ion motion. The insignificance of both factors is proved by observing the saturation of the ion count rate raising both the ion extraction field and the ion acceleration field. The latter measurements are discussed below, but it is of significance here that all ions escaping from the ionization chamber reach the MCP detector because of the large active area of the MCP compared to the width of the bottom electrode aperture and because of the rather high acceleration field. As for the first, the count rate is constant within a relative uncertainty of 0.3% for extraction fields higher than 5 V/cm, for neon ionization both by electrons of different energies and by photons of energies below and above the 1*s* threshold, i.e., energies corresponding to the dominant yield of either singly or doubly charged ions.

As the geometrical dimensions and positions of electron and photon beams may differ, it must also be demonstrated that the ion collection efficiency is constant for different positions of the interaction region within the ionization chamber. To test this, we shift the ionization chamber and MCP detector, both mounted on a linear motion feedthrough, with respect to the ionizing beams. We find the count rates to be constant within 0.4% within a 2.7-mm shift, which, as mentioned above, corresponds to the maximum deviation of the positions of electron and photon beam inside the ionization chamber.

4. Equality of ion detection efficiencies

With the potential configuration used, only ions hitting the holes of the MCP can be detected because all secondary electrons produced by front face collisions are pulled backward from the plate. In this case, the ion detection efficiency, which can be defined as the fraction of the incoming ions that produce detectable pulses at the discriminator output, depends only on the coefficient of the conversion of the ion into secondary electrons, on the gain of the MCPs, and on the threshold level of the amplifier-discriminator combination. Ions formed by EI and PI have different charge spectra and, as a result, different impact energies on the MCP detector. This can lead to different conversion coefficients and to different pulse height distributions at the anode. To obtain equal detection efficiency for all ions created by EI and PI, the ion impact energies must be high enough to guarantee the production of more than one secondary electron for each ion entering a MCP hole and the amplifier-discriminator threshold level has to be low enough to guarantee the detection of each pulse arising at the anode. To meet these requirements, the threshold level is kept as low as possible, providing a cutoff of noise pulses, and the negative potential at the front of the MCP is raised until saturation of the count rate is observed. Figure 2 shows typical dependences of the count rate on the MCP front potential obtained for neon ionization by 1-keV electrons and by photons with energies of 146 and 922.5 eV, corresponding to the dominant yield of either singly or doubly charged ions. In spite of the different behaviors of the saturation curves, which can be explained by different ion collection efficiencies, no change of the count rate is observed within a relative uncertainty of 0.5% for potentials lower than −12 kV.

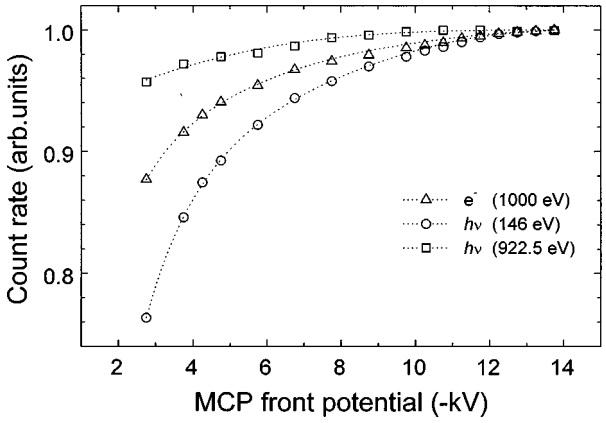

FIG. 2. Count rates observed during neon ionization by 1000-eV electrons and by photons with energies of 146 and 922.5 eV as a function of the MCP front potential. Note that photon energies of 146 and 922.5 eV correspond to the dominant yield of singly and doubly charged ions, respectively.

5. Gas pressure homogeneity and stability

Heterogeneous pressure distribution within the interaction region and pressure drift may lead to unequal conditions for the ion production in two stages of neon ionization. First, the gas inlet valve is located between the turbomolecular pump and the vacuum chamber of the apparatus. With this design, neon atoms get into the vacuum chamber mainly due to a diffusion that leads to a homogeneous distribution within the interaction region. A confirmation of this can be found in the independence of the count rates from the position of the interaction region within the ionization chamber (see Sec. III C 3). To test the influence of pressure drift, neon is ionized several times in succession by electrons and by photons and the count rates normalized to the electron current and to

TABLE II. Measured ratios of total cross sections for electron-impact ionization and photo-ionization in neon and their relative uncertainties (1σ level).

Photon energy $h\nu$ (eV)	$\frac{\sigma_e(E=1000\text{ eV})}{\sigma_{ph}(h\nu)}$	Relative uncertainty of total cross-section ratios(%)
108.1	9.292	1.3
124.0	11.72	1.3
146.1	16.18	1.3
147.2	16.44	1.3
150.1	17.23	1.3
154.9	18.21	1.3
160.2	19.65	1.3
166.9	21.31	1.3
170.2	22.32	1.3
180.2	25.30	1.3
180.8	25.42	1.3
183.4	26.18	1.3
190.2	28.51	1.3
200.2	31.98	1.3
230.3	45.26	1.3
274.4	69.42	1.3
438.7	233.3	1.4
500.9	327.2	1.4
624.9	564.2	1.4
697.1	748.3	1.4
922.5	97.54	1.7
1003.0	123.2	1.7
1103.0	158.4	1.7
1204.0	198.2	1.7
1254.0	218.3	1.7
1304.0	243.8	1.7
1405.0	294.3	1.7
1505.0	345.7	1.7

the photodiode current are measured. We find that the relative uncertainty caused by the gas pressure instability is below 0.1%.

6. Influence of the secondary effects

The fraction of the ion signal caused by secondary effects that are connected with ion scattering and charge-exchange processes as well as with neon ionization by secondary electrons released from the target gas atoms in the ionization process and from the material of the MCP by ion impact depends on the pressure. When these effects are taken into account, Eq. (4) must be transformed, i.e., the cross-section ratio becomes a function of pressure. As an independence of measured cross-section ratios from neon pressure is observed in the working pressure range between 8×10^{-4} Pa and 7×10^{-3} Pa, we find these secondary effects to be insignificant.

Undesired contributions to the ion signals may also result from the ionization by secondary electrons that are released from the material of the gun and the Faraday cup electrodes by electron and photon impact. In addition, a fraction of the ion signal caused by these secondary effects is independent of the pressure. Therefore, in order to estimate the relative uncertainty of the cross-section ratios connected with these effects, either the number of such secondary electrons in the interaction region or the contribution of the latter to the ion signals must be directly determined.

It was discussed before (see Sec. III A) that in the case of EI the number of secondary electrons escaping from both the gun and the Faraday cup electrodes is less than 0.2% of the total electron intensity. We estimate that the upper limit of the contribution to the ion signal is about 0.3% because secondary electrons may have ionization cross sections higher than primary ones. To estimate the contribution of such secondary electrons to the ion signal in the case of PI, a dependence of the count rate on the potential at diaphragm 4 of the electron gun and on the potentials at the cup electrodes is measured. In both cases, no change of the count rate is observed within a relative uncertainty of 0.1%.

D. Contribution from higher-order radiation and stray light

During the PI measurements both the ion count rate and the photodiode current are affected by higher-order radiation and stray light. In some spectral ranges this influence leads to a distortion of the measured cross-section ratios, thus making a correction procedure necessary.

Second-order radiation is predominant in the higher-order spectrum. It always remains below 1% of the total photon flux for all photon energies above 40 eV, except for the region between 110 and 250 eV where no proper filter is installed in the beam line [25]. To reduce second-order radiation in this spectral region, a Mylar filter of approximately 1.5 μm thickness is used. Nevertheless, the remaining second-order contribution still requires a correction, i.e., the measured cross section ratios must be multiplied by the correction factor $K(h\nu)$:

$$K(h\nu)=\frac{\tau(h\nu)+\alpha\tau(2h\nu)\sigma(2h\nu)/\sigma(h\nu)}{\tau(h\nu)+\alpha\tau(2h\nu)\,\eta(2h\nu)/\,\eta(h\nu)}. \qquad (5)$$

In Eq. (5), α is the ratio of second- to first-order photons, $\tau(h\nu)$ [$\tau(2h\nu)$] is the transmittance of the Mylar filter, $\sigma(h\nu)$ [$\sigma(2h\nu)$] is the total PI cross section of neon, and $\eta(h\nu)$ [$\eta(2h\nu)$] is the quantum efficiency of the photodiode for first- [second-] order radiation. We determine the correction factor $K(h\nu)$ using the transmittance of the Mylar filter (which is measured during the cross-section measurements since the filter is mounted on a linear motion feedthrough), well-known PI cross sections (see the Appendix), photodiode quantum efficiencies (see Sec. III B), and ratios α given in [25]. Cross-section measurements are performed at those photon energies only, where the correction is less than 5%, leading to contributions to the relative uncertainty of the measured cross-section ratios of less than 0.5%.

The ratio of the number of stray light photons to the total number of photons is less than 1% in the spectral range below 900 eV, increasing up to 3% at the photon energy of 1500 eV [25]. Use of proper absorption filters suppresses low-energy stray light. In this case, the fraction of the stray light consisting mainly of photons with energies near and in part even above the nominal energy is less than 1% for all photon energies below 1500 eV [25]. This leads to an upper

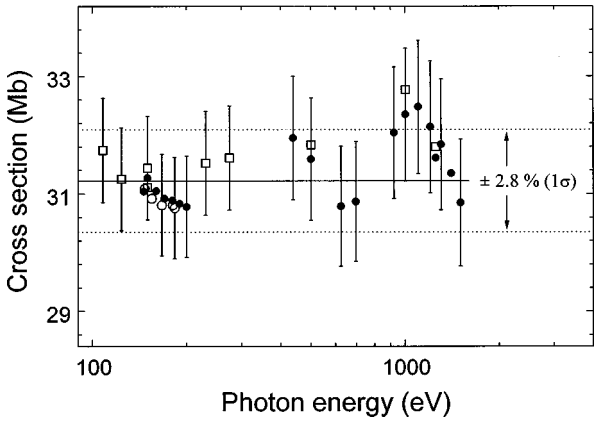

FIG. 3. Total electron-impact ionization cross sections of neon at an electron energy of 1000 eV obtained from measured cross-section ratios by normalization to total photoionization cross sections at different photon energies. Different symbols represent data obtained in three independent periods of measurement at 6-months intervals. The continuous line represents the average value. The representative uncertainty bars at 18 energies correspond to the relative uncertainties mentioned in Sec. IV.

limit of the contribution to the relative uncertainty of our cross-section measurements of 0.2% for photon energies below 700 eV and of 1.0% for photon energies above 900 eV. No measurements are performed in the intermediate spectral range, where the effect of stray light is enhanced by the absorption *K* edge of neon, leading to unacceptable errors.

IV. RESULTS AND DISCUSSION

The ratios $\sigma_e(E)/\sigma_{\mathrm{ph}}(h\nu)$ of total cross sections for EI and PI of neon are measured at an electron energy E of 1000 eV and photon energies $h\nu$ between 100 and 1500 eV in three different periods within 2 yr. The results of these measurements are presented in Table II. The contributions to the total relative uncertainties of the ratios discussed in detail above are summarized in Table I.

The total EI cross section at 1000-eV electron energy deduced from these ratios by normalization to recommended absolute PI cross sections (see the Appendix) is plotted in Fig. 3. The relative uncertainties arise from the relative uncertainties of the measured ratios and the relative uncertainties of the recommended absolute PI cross sections. All data obtained in different periods of measurement agree within the combined uncertainties, demonstrating high reproducibility of our measurements. The measurements at photon energies between 100 and 300 eV result in a total EI cross section $\sigma_e(E=1000\ \mathrm{eV})=31.22$ Mb with a relative uncertainty of 2.8%. Measurements at photon energies between 300 and 1500 eV are affected by slightly higher relative uncertainties of 3.4%. The agreement of our result for $\sigma_e(E=1000\ \mathrm{eV})$ obtained at different photon energies $h\nu$ demonstrates the consistency of our method and its suitability for EI cross-section measurements. In particular, it confirms that our method is unaffected by the severe change in the ion charge spectrum for PI appearing at the 1*s* threshold of neon (see Secs. III C 3 and III C 4).

Next we determine the relative energy dependence of the EI cross sections by comparing ion count rates normalized to the impinging electron current at the reference energy of 1000 eV and at electron energies E between 140 and 4000 eV. The total relative uncertainty of the energy dependence is 1%, arising from contributions from the counting statistics, the determination of the number of impinging electrons, the determination of the electron energy, and the inequality of the interaction path length for electrons of different electron energy.

Finally, using the absolute value for $\sigma_e(E=1000\ \mathrm{eV})$ determined above, we convert the relative energy dependence to absolute total EI cross sections of neon $\sigma_e(E)$ given in Table III. In Fig. 4 we compare these results with published experimental data. The fractional deviation of these data from the present data is also shown to facilitate comparison. The measurements of Schram *et al.* [7], Gaudin and Hage-

TABLE III. Total electron-impact ionization cross sections of neon $\sigma_e(E)$ and their relative uncertainties.

Electron energy E (eV)	$\sigma_e(E)$ (Mb)	Relative uncertainty (%)
140	65.02	3.0
150	65.41	3.0
160	65.59	3.0
170	65.66	3.0
180	65.41	2.9
200	64.78	2.9
225	64.06	2.9
250	62.41	2.9
300	59.25	2.9
350	55.94	2.9
400	52.82	2.9
450	50.23	2.9
500	47.48	2.9
550	45.21	2.9
600	43.11	2.9
650	41.14	2.9
700	39.30	2.9
750	37.64	2.9
800	36.22	2.9
850	34.78	2.9
900	33.47	2.9
950	32.26	2.9
1000	31.22	2.8
1100	29.28	2.9
1200	27.55	2.9
1300	26.03	2.9
1400	24.69	2.9
1500	23.54	2.9
1600	22.48	2.9
1700	21.41	2.9
1800	20.60	2.9
1900	19.79	2.9
2000	19.07	2.9
2500	16.05	2.9
3000	13.96	2.9
3500	12.34	2.9
4000	11.16	2.9

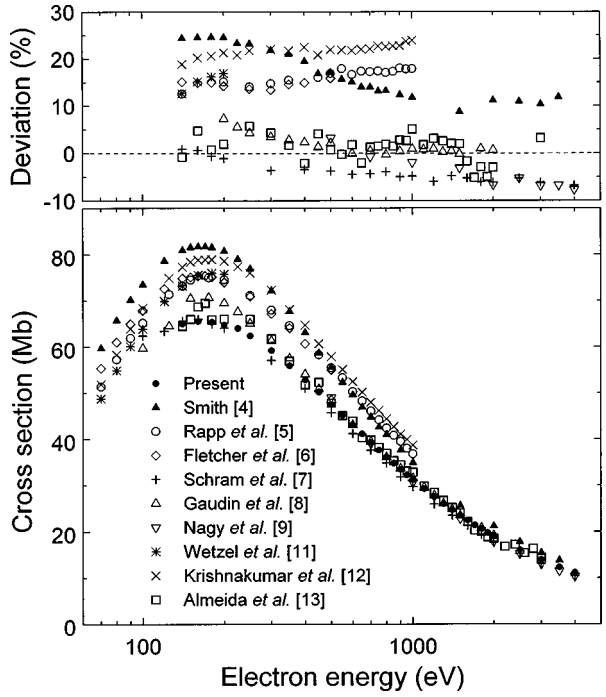

FIG. 4. Present total electron-impact ionization cross sections of neon compared with other experimental data [4–9,11–13]. The upper plot shows the fractional deviation of these data from the present data.

mann [8], and Nagy, Skutlartz, and Schmidt [9] provide total ionization cross sections, whereas those of Smith [4], Rapp and Englander-Golden [5], and Fletcher and Cowling [6] provide gross ionization cross sections σ_{gross} [14]. We recalculate these data to total ionization cross sections σ_e using ratios $\sigma_{\text{gross}}/\sigma_e$ reported by De Heer, Jansen, and Van der Kaay [27] with relative uncertainties of less than 1%. Wetzel *et al.* [11] measured single-ionization cross sections σ^+ [14] and then calculated total ionization cross sections σ_e using ratios σ^+/σ_e taken from the literature. Krishnakumar and Srivastava [12] and Almeida, Fontes, and Godinho [13] normalized their relative measurements to absolute cross sections reported in [5].

Figure 4 reveals considerable discrepancies in the absolute cross-section data reported by different experimental groups that often exceed the combined uncertainties. Undoubtedly, one of the most significant sources of these discrepancies is connected with the measurements of the target gas density. For example, the results obtained by Rapp and Englander-Golden [5] and by Schram *et al.* [7] reveal discrepancies of up to 24%, though the authors have claimed relative uncertainties of 7% and 6%, respectively. Both groups used a similar technique based on the measurement of the total ion yield produced by an electron beam passing through a well-defined length of gas in a beam-static-gas configuration. The only significant difference was the method by which the target gas density was determined. Schram *et al.* [7] used a wall-cooled McLeod gauge corrected for the mercury pumping effect and Rapp and Englander-Golden [5] used an effusive-flow apparatus calibrated against pressure measurements in molecular hydrogen made with a McLeod gauge.

Other experimental data [4,6,8,9,11] do not clear up the situation. Especially at electron energies above 300 eV, these data tend to agree with the results of either Rapp and Englander-Golden [5] or Schram *et al.* [7], but they do not agree with one another. Fletcher and Cowling [6] obtained cross sections with a claimed relative uncertainty of 4.5% using an apparatus similar to that of Rapp and Englander-Golden [5], but they measured the target gas pressure with an ionization gauge calibrated against a capacitance diaphragm gauge. Incidentally, the results of these two groups are in close agreement. The early measurements of Smith [4], who used a McLeod gauge uncorrected for the mercury pumping effect, are also very similar to those of Rapp and Englander-Golden [5]. The measurements of Wetzel *et al.* [11] carried out by a crossed fast-neutral-beam–electron-beam technique confirm again those of Rapp and Englander-Golden [5], although with a relative uncertainty of 15% claimed by the authors, this is not a stringent statement. The absolute cross sections reported by Gaudin and Hagemann [8] and Nagy, Skutlartz, and Schmidt [9] with a relative uncertainty of 10% agree within their experimental uncertainties with those of Schram *et al.* [7]. Both groups used similar techniques based on a separation and absolute registration of the differently charged ions formed by EI along a known length, but measurements of the gas pressure were made with ionization gauges calibrated against a McLeod gauge and a capacitance diaphragm gauge, respectively.

The present measurements are free of errors associated with the absolute pressure measurement. Our data agree with those of Schram *et al.* [7], Gaudin and Hagemann [8], and Nagy, Skutlartz, and Schmidt [9] within the combined uncertainties, but the values are significantly lower than the results of Smith [4], Fletcher and Cowling [6], and Rapp and Englander-Golden [5]. The latter difference is of particular importance because the results of Rapp and Englander-Golden [5] were considered *de facto* as a standard and were often used to normalize relative partial ionization cross sections.

Surprisingly, even the relative measurements of the energy dependence of EI cross sections carried out by different groups exhibit differences. Our results agree very well with those of Fletcher and Cowling [6]. Relative energy dependences of cross sections reported by Schram *et al.* [7], Rapp and Englander-Golden [5], Gaudin and Hagemann [8], and Krishnakumar and Srivastava [12] with relative uncertainties below 2% agree with our results in the electron energy range above 250 eV, while discrepancies of up to 6% exist for energies near the cross-section maximum. More considerable discrepancies of up to 11% exist between our data and those of Smith [4], and Nagy, Skutlartz, and Schmidt [9]; their data decrease more rapidly than ours with increasing electron energy. The relative measurements recently carried out by Almeida, Fontes, and Godinho [13] agree with our relative measurements, although a random scattering of up to 6% exists between the two data sets.

Comparison with theory

In Fig. 5 our total cross-section data for EI of neon are plotted together with calculated data. The fractional deviation from the present data are also given to facilitate comparison. The figure shows recent results of Chang and Altick [28] using the distorted-wave Born approximation, of Kim

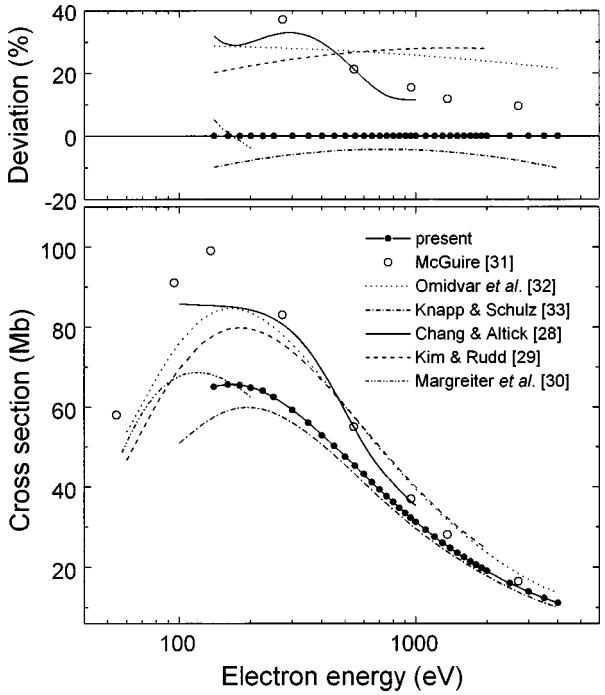

FIG. 5. Present total electron-impact ionization cross sections of neon compared with theoretical calculations [28–33]. The upper plot shows the fractional deviation of these data from the present data.

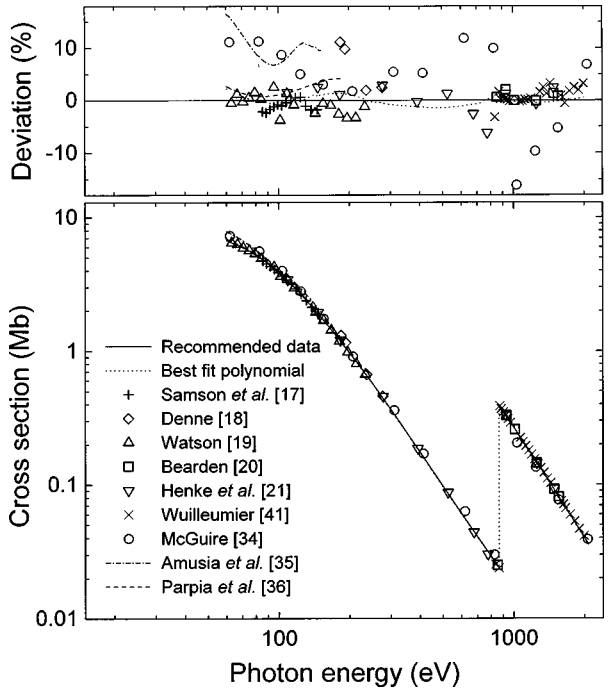

FIG. 6. Total photoionization cross sections of neon: recommended data, calculation by the best fit polynomial, experimental data [17–21,41] included in the present compilation (the data of [37,39,40] are not shown), and theoretical [34–36] calculations. The upper plot shows the fractional deviation of these data from the recommended data.

and Rudd [29] using the binary-encounter-dipole model, and of Margreiter, Deutsch, and Märk [30] using a semiclassical approach. Moreover, we show three different calculations within Born approximation made by McGuire [31], Omidvar, Kyle, and Sullivan [32], and Knapp and Schulz [33]. Only the results of the latter as well as of Margreiter, Deutsch, and Märk [30] are in good agreement with our experimental data. We do not go into a detailed comparison of the theoretical approaches, but we note that Knapp and Schulz [33] are the only ones who take into account the exchange between the ejected electron and the bound ones. The other quantum-mechanical calculations overestimate our data by up to 40%, indicating that the exchange effect is not negligible in the case of EI.

In addition, we note here that, in contrast to EI, the exchange effect is of less influence on the calculation of PI cross sections (at least far from ionization thresholds) because of a rather high energy of the ejected electron. Indeed, in Fig. 6 we compare the experimental PI data (see the compilation in the Appendix) with the results of the dipole approximation calculation of McGuire [34], the random-phase approximation with exchange calculation of Amusia, Cherepkov, and Chernysheva [35], and the relativistic time-dependent local-density approximation calculation of Parpia, Johnson, and Radojevic [36] and find close agreement. In addition, we emphasize a very good agreement between the experimental data and theoretical data of McGuire (at least in the spectral range from 100 to 600 eV), who used the same method in his calculation of PI [34] and EI [31] cross sections, neglecting the exchange between the ejected electron and bound ones. This demonstrates that additional efforts are necessary not only from the experimental but also from the theoretical side to obtain a consistent and well-known set of EI cross sections as is already available for PI data.

V. CONCLUSION

We describe a method and an apparatus for measuring total EI cross sections of rare gases. The method is based on the direct comparison of total EI cross sections and PI cross sections, the latter presently known with relative uncertainties as low as 1% to 3%, and on two main instrumental developments. The first is associated with a highly accurate device for soft-x-ray and vacuum ultraviolet photon flux measurements: a cryogenic electrical substitution radiometer providing a relative uncertainty of the radiation intensity below 1%. The other development is an upgraded ionization chamber for the comparison of total ion yields in EI and PI. As a result, relative uncertainties as low as 1.3% to 1.7% were achieved in our measurements of EI and PI cross-section ratios. Our measurements eliminate the main uncertainties inherent in early cross-section measurements and yield a common scale of total cross sections for EI and PI. Using the measured ratios and well-known PI cross sections, we deduce EI cross sections of neon with the relative uncertainty of 2.8% at an electron energy of 1000 eV and of less than 3.0% at all other energies ranging from 140 to 4000 eV. Our results considerably improve the data base for absolute total EI cross sections and hence for partial cross sections derived from these data.

ACKNOWLEDGMENTS

The authors are grateful to F. Scholze for fruitful discussions. This work was funded by the Deutsche Forschungsge-

meinschaft (Grant No. N436 RUS 100/95), by the Russian Foundation for Basic Research (Grant No. 96-02-00203G), and partly by the NATO Networking Infrastructure (Grant No. CN. NIG 96 0544).

APPENDIX: TOTAL PHOTOIONIZATION CROSS SECTIONS OF NEON

Reviews of PI cross sections were presented by West and Marr [37] and Henke, Gullikson, and Davis [38]. Since then, several studies of PI cross sections were reported [16,17,39]. In this work we compile data published for the photon energy range from 70 to 2000 eV, i.e., in the spectral interval of interest here. We select PI cross section values according to the following criterion: The cross sections were measured after 1960 with quoted relative uncertainties better than 7%, using all available experimental methods [15]. Accordingly, we use data obtained by the absorption cell technique [18–21,37,40,41], the double-ionization chamber technique [17], and the high-resolution dipole (*e*,*e*) method using Thomas-Reiche-Kuhn sum-rule normalization of the Bethe-Born-converted electron-energy-loss spectrum [39].

Recommended values for PI cross sections $\sigma_{\mathrm{ph}}(h\nu)$ are obtained from a polynomial fit to each set of original experimental values $\sigma_i(h\nu)$ by the least-square method, followed by a weighted averaging of these fits according to Eq. (A1). The weights $W_i(h\nu)$ are determined as a square root from a sum of squares of the relative uncertainties claimed by the authors and the scattering of the original experimental values around their average values

$$\sigma_{\mathrm{ph}}(h\nu)=\frac{\Sigma_i[\sigma_i(h\nu)/W_i^2(h\nu)]}{\Sigma_i[1/W_i^2(h\nu)]}. \tag{A1}$$

TABLE IV. Coefficients of the best polynomial fit of experimental photoionization cross-section data of neon.

Coefficient	70 eV$<h\nu<$870 eV	871 eV$<h\nu<$2000 eV
A_0	−9.983	5.795
A_1	15.62	−1.573
A_2	−6.918	−0.1835
A_3	0.8749	0

The relative uncertainties of the recommended data are 2.5% at photon energies between 70 and 300 eV and approximately 3% at photon energies between 300 and 2000 eV.

Having obtained the recommended values, we fit them by the least-square method with a Taylor polynomial. Briefly, the dependence of the PI cross section $\sigma_{\mathrm{ph}}(h\nu)$ (in Mb) on the photon energy $h\nu$ (in eV) can be represented as

$$\ln\,\sigma_{\mathrm{ph}}(h\nu)=\sum_{i=0}^{3} A_i[\ln\,h\nu]^i. \tag{A2}$$

The coefficients A_i are given in Table IV for the spectral regions below and above the 1*s* threshold of neon (~870 eV).

Figure 6 shows the recommended values for total PI cross sections of neon together with selected experimental data employed for the compilation (shown are only experimental data obtained with relative uncertainties of 2% to 5%), the best fit curve calculated from Eq. (A2), and the results of theoretical calculations mentioned in Sec. IV A. The fractional deviation of these data from the recommended values is also shown in the upper part of Fig. 6.

[1] L. J. Kieffer and G. H. Dunn, Rev. Mod. Phys. **38**, 1 (1966).
[2] T. D. Märk and G. H. Dunn, *Electron Impact Ionization* (Springer, Berlin, 1985).
[3] K. H. Becker and V. Tarnovsky, Plasma Sources Sci. Technol. **4**, 307 (1995).
[4] P. T. Smith, Phys. Rev. **36**, 1293 (1930).
[5] D. Rapp and P. Englander-Golden, J. Chem. Phys. **43**, 1464 (1965).
[6] J. Fletcher and I. R. Cowling, J. Phys. B **6**, L258 (1973).
[7] B. L. Schram, F. J. De Heer, M. J. Van der Wiel, and J. Kistemaker, Physica (Amsterdam) **31**, 94 (1965); B. L. Schram, A. J. H. Boerboom, and J. Kistemaker, *ibid.* **32**, 185 (1966); B. L. Schram, *ibid.* **32**, 197 (1966); B. L. Schram, H. R. Moustafa, J. Schutten, and F. J. De Heer, *ibid.* **32**, 734 (1966).
[8] A. Gaudin and R. Hagemann, J. Chime Phys. **64**, 1209 (1967).
[9] P. Nagy, A. Skutlartz, and V. Schmidt, J. Phys. B **13**, 1249 (1980).
[10] H. C. Straub, P. Renault, B. G. Lindsay, K. A. Smith, and R. F. Stebbings, Phys. Rev. A **52**, 1115 (1995).
[11] R. C. Wetzel, F. A. Baiocchi, T. R. Hayes, and R. S. Freund, Phys. Rev. A **35**, 559 (1987).
[12] E. Krishnakumar and S. K. Srivastava, J. Phys. B **21**, 1055 (1988).
[13] D. P. Almeida, A. C. Fontes, and C. F. L. Godinho, J. Phys. B **28**, 3335 (1995).
[14] Total ionization cross sections discussed in the present paper are the sum of partial cross sections σ^{n+} for the production of ions with charge *n*, i.e., $\sigma_e=\Sigma\sigma^{n+}$. In the case of EI, these cross sections are often called counting ionization cross sections. In contrast, gross ionization cross sections are a charge-weighted sum of partial cross sections, i.e., $\sigma_{\mathrm{gross}}=\Sigma n\sigma^{n+}$.
[15] J. A. R. Samson, Phys. Rep., Phys. Lett. **28C**, 303 (1976).
[16] J. A. R. Samson and L. Yin, J. Opt. Soc. Am. B **6**, 2326 (1989).
[17] J. A. R. Samson, L. Lyn, G. N. Haddad, and G. C. Angel, J. Phys. IV **1**, C1 (1991).
[18] D. R. Denne, J. Phys. D **3**, 1392 (1970).
[19] W. S. Watson, J. Phys. B **5**, 2292 (1972).
[20] A. J. Bearden, J. Appl. Phys. **37**, 1681 (1966).
[21] B. L. Henke, R. L. Elgin, R. E. Lent, and R. B. Ledingham, Norelco Reporter **14**, 112 (1967).
[22] S. V. Bobashev and L. A. Shmaenok, Rev. Sci. Instrum. **52**, 16 (1981).
[23] H. Rabus, V. Persch, and G. Ulm, Appl. Opt. **36**, 5421 (1997).
[24] F. Scholze, H. Rabus, and G. Ulm, Appl. Phys. Lett. **69**, 2974 (1996).

[25] F. Scholze, M. Krumrey, P. Müller, and D. Fuchs, Rev. Sci. Instrum. **65**, 3229 (1994).
[26] N. Saito and I. H. Suzuki, Int. J. Mass Spectrom. Ion Processes **115**, 157 (1992).
[27] F. J. De Heer, R. H. J. Jansen, and W. Van der Kaay, J. Phys. B **12**, 979 (1979).
[28] D. W. Chang and P. L. Altick, J. Phys. B **29**, 2325 (1996).
[29] Y. K. Kim and M. E. Rudd, Phys. Rev. A **50**, 3954 (1994).
[30] D. Margreiter, H. Deutsch, and T. D. Märk, Int. J. Mass Spectrom. Ion Processes **139**, 127 (1994).
[31] E. J. McGuire, Phys. Rev. A **3**, 267 (1971).
[32] K. Omidvar, H. L. Kyle, and E. C. Sullivan, Phys. Rev. A **5**, 1174 (1972).
[33] E. W. Knapp and M. Schulz, J. Phys. B **7**, 1875 (1974).
[34] E. J. McGuire, Phys. Rev. **175**, 20 (1968).
[35] M. Ya. Amusia, N. A. Cherepkov, and L. V. Chernysheva, Zh. Eksp. Teor. Fiz. **60**, 160 (1971) [Sov. Phys. JETP **33**, 90 (1971)].
[36] F. A. Parpia, W. R. Johnson, and V. Radojevic, Phys. Rev. A **29**, 3173 (1984).
[37] J. B. West and G. V. Marr, Proc. R. Soc. London, Ser. A **349**, 397 (1976).
[38] B. L. Henke, E. M. Gullikson, and J. C. Davis, At. Data Nucl. Data Tables **54**, 181 (1993).
[39] W. F. Chan, G. Cooper, X. Guo, and C. E. Brion, Phys. Rev. A **45**, 1420 (1992).
[40] D. L. Ederer and D. H. Tomboulian, Phys. Rev. **133**, A1525 (1964).
[41] F. Wuilleumier, Ph.D. thesis, Université de Paris, 1969 (unpublished).